2-2017

Experiments on the Low Frequency Barrier Characteristics of Cellular Metamaterial Panels in a Diffuse Sound Field

Srinivas Varanasi
Purdue University, v.s.s.srinivas@gmail.com

J Stuart Bolton
Purdue University, bolton@purdue.edu

Thomas Siegmund
Purdue University, siegmund@ecn.purdue.edu

Experiments on the Low Frequency Barrier Characteristics of Cellular Metamaterial Panels in a Diffuse Sound Field

Srinivas Varanasi

School of Mechanical Engineering, 585 Purdue Mall,

West Lafayette, IN 47907-2088, U.S.A.

J. Stuart Bolton

Ray W. Herrick Laboratories, School of Mechanical

Engineering, Purdue University, 177 Russell Street,

West Lafayette, IN 47907-2099, U.S.A.

Thomas Siegmund

School of Mechanical Engineering, 585 Purdue Mall,

West Lafayette, IN 47907-2088, U.S.A.

Note: This article was published in the Journal of the Acoustical Society of America.

Citation: J. Acoust. Soc. Am. 141, 602 (2017); doi: 10.1121/1.4974257

View online: http://dx.doi.org/10.1121/1.4974257

Abstract

The metamaterial under investigation here consists of a periodic arrangement of unit plates in a grid-like frame such that there is a contrast in the local areal mass between cell interior and cell wall. In the low frequency range and under normal incidence this metamaterial panel exhibits a sound transmission loss significantly larger than the transmission loss of an unstructured panel with the same homogeneous mass per unit area. However, when the incident sound field is diffuse, the relative advantage of the metamaterial barrier is reduced or eliminated. A sequence of experiments is documented to demonstrate that the relative advantage of the metamaterial barrier can be realized even in a diffuse sound field by creating a hybrid barrier system which embeds the metamaterial layer between a normalizing waveguide layer on the incident side and an absorbing layer on the transmitted side. The sound normalizing waveguide layer is a lattice structure, and the absorbing layer is high performance glass fiber mat. By using measurements of the transmission loss of a 1.2 m square panel system the role of each of these components is demonstrated.

Keywords:

Planar cellular metamaterial; Diffused sound field; Barrier materials; Sound transmission loss

Nomenclature

c : Sound speed in air

f : Frequency of sound waves

I_0 : Intensity of the incident sound field

I_t : Intensity of the transmitted sound field

L_0 : Edge length of the panel overall

L_p : Edge length of the interior of the unit cell

L_t: Long transverse dimension of a rectangular waveguide

SAL: Sound absorbing layer

SNL: Sound normalizing layer

STL: Sound transmission loss

$\mathrm{STL_n}$: Sound transmission loss in a normally incident sound field

$\mathrm{STL_d}$: Sound transmission loss in a diffuse sound field

t_f : Thickness of the unit cell wall

$mean\,(t_p)$: Measured mean thickness of the unit cell interior

$stdev\,(t_p)$: Standard deviation of the measured unit cell interior thickness

t_p : Thickness of the unit cell interior

W_f : Width of the unit cell wall

θ : Angle of incidence of sound field

μ : Ratio of mass of the unit cell wall to the unit cell interior

ρ_0 : Mass density of air

σ : Areal mass density

I. Introduction

The control of low frequency audible air-borne noise produced by, for example, aircraft [1] or home appliances [2] is an important engineering task. To effectively control the transmission of sound, conventional barrier materials require high mass per unit area since sound transmission is controlled by inertia in the low frequency region [3]. Metamaterials potentially offer solutions that address the challenge of controlling sound transmission with low mass. Prior investigations on relevant metamaterial systems have considered material configurations such as a matrix with embedded resonating elements, typically a heavy mass coated with a soft rubber coating [4, 5], membrane-based materials [6, 7], and plate based materials [8, 9]. Prior studies on acoustic metamaterials for sound barriers were performed employing either analytical or computational methods: for a review see [10]. Related experiments [4, 7, 11, 12, 13, 14, 15] made use of bench-top setups to observe the barriers' sound transmission loss characteristics under normal incidence. This method is typically used to characterize sound absorbing materials [16, 17, 18]. There are also a few investigations involving sound source excitation with alternate experimental approaches [19, 20, 21, 22], but these are also limited to normal incidence, one-dimensional wave propagation. While the work in references [4, 7, 12, 13, 14, 15] focused on determining the sound transmission loss behavior of the proposed materials, particularly in the low audible frequency range, the work reported in references [19, 20, 21, 22] primarily considered the verification of theoretical con-

cepts of effective negative density, modulus and the co-existence of locally resonant band gaps and Bragg band gaps. Thus, almost all prior research has been concerned with barrier material subjected to a normally incident sound field. However, sound fields are seldom unidirectional [3, 23]. Investigations of conventional barrier materials have found that their STL values in a diffuse field are generally 5 dB lower than those in a normally incident sound field [3]. Therefore a need exists to understand the behavior of cellular metamaterials for varying levels of diffuseness of the sound field. Such investigations require large-scale experiments and no longer can be conducted in the standing wave tube set-up. Only a few prior investigations of this kind have been reported. In Xiao et al. [8] and in Assouar et al. [24] the behavior of metamaterial plates with attached resonators was studied by using the methods of plane wave expansion and effective media. These authors predicted that the sound transmission loss in a diffuse sound field would be lower than in a normally incident sound field. Hall et al. [25] reported diffuse field experiments on metamaterial-based sound treatments but no details were provided about the metamaterial construction.

In this paper, intensity-based sound transmission loss experiments are described in which planar cellular metamaterials [9], Fig. 4, were subjected to incident sound fields using a reverberation room setup [26, 27]. The present paper expands on preliminary data previously presented by the authors [29]. Two application-scale planar cellular panels were constructed so that two different characteristic resonance frequencies could be considered. STL data for the two metamaterial panels were compared to that of representative

limp panels. A hybrid panel system was then considered in which a sound normalizing layer (a waveguide) was added on the incident side of the panel and a sound absorbing layer was added on the transmitted side of the panel. The resulting hybrid barrier system was found to be a more mass-efficient solution when compared to conventional sound barriers, particularly at low frequencies. Finally, experimentally determined STL data for the metamaterial panels were compared to predictions from a unit cell numerical model [9].

II. Materials

Six materials systems were considered: (1) cellular metamaterial panels alone (two configurations), (2) cellular metamaterial panel with a sound normalizing layer on the incident side, (3) cellular panels with a sound normalizing layer on the incident side and a sound absorbing layer on the transmitted side (referred to as Hybrid Metamaterial Panel - HMP), (4) a limp panel alone, (5) a limp panel with a sound normalizing layer on the incident side, and (6) a limp panel with a sound normalizing layer on the incident side and a sound absorbing layer on the transmitted side (referred to as Hybrid Conventional Panel - HCP). Figure 1 shows schematic drawings for the cellular panel based materials systems and Fig. 2 for the reference limp panel materials systems. Figure 3 depicts photographs of the cellular panel based systems.

Details of the cellular panel geometry are given in Fig.4. Optically clear, cast-acrylic plastic stock (McMaster-Carr) was used to construct the cellular metamaterial panel. Cells were machined into the stock plate using a CNC

Router. The cast acrylic possesses an elastic modulus of 3.04 GPa, a Poisson's ratio of $\nu = 0.43$ (upper bound value) and a density of $\rho = 1.18$ g/cm^3. The panels possess a square shape of edge length $L_0 = 1.22$ m. The cellular panels consisted of 18×18 square unit cells. The unit cells dimension $L_p + 2W_f = 63.0$ mm was motivated by the cross-sectional dimensions of a standing wave tube apparatus used previously [16]. Two planar cellular metamaterial panel configurations [9] were studied and characterized by the ratio μ of mass of the unit cell wall to that the cell interior. The configuration named $Design1$ possessed $\mu = 2.1$ while for the configuration $Design2$ the value wass $\mu = 3.5$. For $Design1$ and $Design2$ the thickness of the unit cell interior plate was $mean\,(t_p) = 2.99$ and 1.81 mm with a $stdev\,(t_p)$ of 0.31 and 0.45 mm, resulting in an averaged mass per unit area of $\sigma = 6.93$ and 5.78 kg/m^2, respectively.

An aluminum panel (Al alloy 1100) of average thickness 2.35 mm was used as a representative conventional limp panel. Its averaged mass per unit area of $\sigma = 6.14$ kg/m^2 fell between that of the two cellular panel configurations.

The sound normalizing layer (SNL) possesses a thickness of 101.6 mm and consists of an array of square unit cells with an edge length of 63.5 mm and a wall thickness of 3.175 mm. The layer was constructed from balsa wood strips in a square lattice structure. This layer acts as a waveguide causing the sound in each cell to approach the cellular panels at normal incidence [30]. Because of the finite cross-section dimension of the cells, higher order modes may propagate within each cell, and each of those modes has a characteristic cutoff frequency. For sound frequencies below the cut-off frequency of the

lowest non-zero mode, i.e., $c/2L_t$ where c is the speed of sound in air and L_t is the longer transverse dimension of a rectangular waveguide, only plane waves can propagate along the duct axis. For the present waveguide configuration, a plane wave field is theoretically present for sound waves below 2700 Hz.

The sound absorbing material comprising the sound attenuation layer (SAL) consisted of two layers of a 1 inch thick glass fiber blanket (Johns Manville Corp., Microlite AA Noise Reduction Blankets) with $\sigma_{mat} = 0.4064\,\mathrm{kg/m^2}$.

Note that the overall assembly is an extended reaction system. The normalizing layer is locally reacting below 2700 Hz since, by its physical nature it prevents sound propagation parallel to the surface of the cellular panel in that frequency range. Thus, the combination of the normalizing layer and the cellular panel is approximately locally reacting in that frequency range, but it is only approximately locally reacting since the SAL and the subsequent air space behind the cellular panel are themselves not locally reacting.

III. Methods

A. Experiments

An intensity-based method [27] was used to measure the sound transmission loss. The experimental setup is shown schematically in Figs. 5 and 6. The experimental set-up follows the guidance of [28] but goes beyond the diffuse sound field considered in the standard. The set-up consists of a reverberation room (volume of $254.9\,\mathrm{m^3}$) and a semi-anechoic enclosure connected through

a window (L_0 by L_0) into which the test samples were placed. Hard concrete walls surround the reverberation room. Noise was generated inside the reverberation room by two loudspeakers (Altec Lansing Model 902 - 8A/B). The speakers were initially positioned such that a diffuse sound field was created through multiple reflections by the hard concrete walls, Fig. 5. In an alternate arrangement, the loudspeakers were oriented parallel to the test panel to create a nominally normal incident sound field, Fig. 6).

The speakers were connected to two independent random white noise signals generated by the Brüel and Kjær (B&K) Pulse Labshop software interface. The signals had a frequency span of 6.40 kHz with their center frequency being 3.20 kHz, and they were amplified by a QSC Model 1080 stereo amplifier. A microphone (B&K pre-polarized free field 1/2-inch, Type 4189) was stationed in the reverberation room to monitor the sound pressure level inside the room.

The test panels were fixed in the window by two wooden frames on either side of the panel which were in turn tightly held in place by clamps anchored in the room walls. The frame inside the reverberation room was permanently fixed and only the frame facing the anechoic termination was operated when exchanging specimens. The part of the panel held by the frames was immovable and therefore it was assumed not to contribute towards the observed sound transmission loss. The effective area of the panel exposed to the incident sound field was hence 1.134 by 1.134 m. The panel was sealed along its edges by using an adhesive tape and modeling clay to prevent air leaks from corrupting the intensity probe measurements.

The semi-anechoic enclosure was an assembly of movable walls, having thick wedges of absorbing material, that enclosed the window holding the test specimen. A sound intensity probe consisting of a pair of 1/2-inch B&K Type 4197 microphones physically separated by a spacer of size 12 mm was used to measure the sound intensity normal to the test panel. This setup provides reliable measurements of sound intensity up to a frequency of 5 kHz [31]. A square array of twenty five uniformly spaced probe positions was used to sample the intensity of sound spanning the full panel. The measurements were taken at a distance of 12.7 cm (5 in.) from the panel on the anechoic enclosure side.

At the start of each experiment, the microphone and the intensity probe were calibrated. The microphone was calibrated using a B&K Type 4231 sound source. The intensity probe was calibrated for pressure, velocity and intensity measurements using a B&K Type 3541-A calibrator consisting of a pistonphone sound source (B&K Type 4228) and a coupler. The pressure-intensity index was checked using a white noise source (B&K Type ZL0055) and the coupler from the B&K calibrator Type 3541. The sound pressure level inside the reverberation room was monitored during each experiment and an overall sound pressure level (SPL) of 105 dB was maintained in the reverberation room. Sound intensity (I_0) was first measured at the twenty five probe positions *without* the panel in place to determine the intensity of sound incident on the test panel. Next, the panel was clamped in the window with the open cell side facing the incident sound field and sound intensity (I_t) was measured again at the probe positions to determine the sound intensity on

the transmitted side. The sound intensity spectrum was measured in $1/12^{th}$ octave bands with the lower and upper center frequencies being 19.31 Hz and 6.131 kHz, respectively. Sound intensities I_0 and I_t averaged over the twenty five probe points were used to calculate the averaged STL:

$$\mathrm{STL} = -10\log_{10}(\|I_t/I_0\|). \tag{1}$$

B. Analytical Expression for the STL of Limp Panels

For a limp panel with a mass per unit area of σ the sound transmission loss in a diffuse field is (STL_d) and that in a normal sound field (STL_n) are calculated as [3]:

$$T(\theta) = \frac{2\rho_0 c}{2\rho_0 c + j\omega\sigma\cos(\theta)}, \tag{2a}$$

$$\tau(\theta) = \|T(\theta)\|^2 = \frac{4{\rho_0}^2 c^2}{4{\rho_0}^2 c^2 + \omega^2\sigma^2\cos(\theta)^2}, \tag{2b}$$

$$\bar{\tau} = 2\int_0^{90^\circ} \tau(\theta)\sin(\theta)\cos(\theta)\,\mathrm{d}\theta, \tag{2c}$$

$$\mathrm{STL}_d = -10\log_{10}(\bar{\tau}), \tag{2d}$$

$$\mathrm{STL}_\mathrm{n} = -10\log_{10}[\tau(0)]. \tag{2e}$$

Here, θ is the angle of incidence of a sound wave, ρ_0 is the density of air, c is the speed of sound in air, $\omega = 2\pi f$ where f is the frequency in Hz, and $\tau(\theta)$ is the plane wave transmission coefficient of a limp panel with an areal mass σ for a sound wave incident at an angle θ.

C. Computational Approaches

Numerical models of the unit cells of the cellular panels subjected to a normally incident sound field were employed to further investigate the sound transmission loss observations. STL values were predicted using a representative unit cell model [9] and the ABAQUS FE code [32]. The geometric dimensions of the models and the elastic properties corresponded to the averaged values of the measured quantities. The numerical analysis was based on a steady-state, dynamically-coupled structural-acoustic procedure. The details of the finite element model are given in Appendix A. A numerical-experimental validation of that acoustical analysis was described in [9].

IV. Results and Discussion

Figures 7 to 9 depict results for measurements of STL in the diffuse sound field. In those figures, the data for panels alone and panels in combination with the sound normalizing layer (SNL) are shown. Experimental data are compared to the predicted $\mathrm{STL_d}$ and $\mathrm{STL_d}$ values given by Eq. 2, always using the corresponding σ values. All plots depicting STL data consider a frequency range between 100 and 4500 Hz. The frequency axis is on log scale with major intervals representing 1.0 kHz and the minor intervals each 200 Hz.

The measured STL for the bare *reference limp panel*, Fig. 7, predominantly follows the analytically predicted behavior of a limp panel in a purely diffused sound field, Eq. 2d. The measured and predicted sound transmission

loss values were found to deviate from each other in two instances. For frequencies around 1000 Hz, the discrepancy between measured and predicted sound transmission loss is attributed to resonance conditions associated with the test window dimensions, particularly its depth. For frequencies above 4000 Hz, the deviation of the experimenal data from Eq. 2d is attributed to the coincidence phenomenon [3]. The coincidence frequency for the reference limp panel is around 5700 Hz. As the coincidence frequency (>5000 Hz here) is significantly above the frequency of the local resonance of the cellular panel, the STL predictions in this paper were developed without accounting for the coincidence effect. The first flexural frequency of the whole panel occurs well below 300 Hz and therefore, the edge conditions of the panel do not play a significant role beyond 300 Hz, the valid region for the experimental setup. The reference limp panel with the sound normalizing layer added on the incident sound side resulted in a measured STL higher than that of of the bare reference limp panel for $f > 500$ Hz, Fig. 7. For 500 Hz $\leqslant f \leqslant 2500$ Hz the measured STL data approach those of the analytically predicted behavior of a limp panel in a normally incident sound field, Eq. 2e. For even higher frequencies the reduction in STL is again attributed to the coincidence effect.

Considering the characteristics of the cellular panel with the sound normalizing layer, once again a significant increase in the STL was observed: Fig. 8. For the bare *cellular metamaterial panels* the measured sound transmission loss was expected to follow the predicted STL_d only at low frequencies. Instead, at higher frequencies a local peak and dip associated with the

resonance and antiresonance inherent to the metamaterial [9] was expected.

For the metamaterial panel $Design1$, Fig. 8, the measured STL values did not exhibit a significant alignment with that expected response. The local increase in the STL value at 1000 Hz for the panels alone (attributed to the test window dimensions) is broadened. Elevated STL values were found between 800 Hz and 1500 Hz and are again attributed to resonance conditions associated with the test window, rather than the metamaterial structure. At 3000 Hz a dip in STL was found but there was no associated peak in the STL before 3000 Hz. This STL dip at 3000 Hz is not associated with the coincidence phenomenon as the coincidence frequency for an σ-equivalent limp panel made of the same material occurs above 5000 Hz. It is rather attributed to the cellular resonance/antiresonance response, but the expected corresponding beneficial STL sound was not well observed in the panel $Design1$ response. The addition of the SNL raised the STL for frequencies higher than 800 Hz, but caused little to no change of the STL in the resonance/antiresonance domain near 3000 Hz. In summary, for the bare metamaterial panel $Design1$, the resonance/anitresonance response observed at normal incidence was not reproduced in a diffuse sound field.

For the metamaterial panel $Design2$, however, the expected peak-dip response was observed: Fig. 9. The panel $Design2$ possesses a 16 percent lower averaged mass per unit area compared to $Design1$ and a 6 percent lower value compared to the reference limp panel. Yet, the panel $Design2$ possesses a larger mass ratio between cell wall and interior than panel $Design1$: i.e., $\mu_2 = 3.5$ compared to $\mu_1 = 2.1$. When this panel was subjected to a diffuse

sound field, a pronounced peak in the STL occured in the frequency range of $1200 - 1400$ Hz along with an associated STL dip in the frequency range from 1500 to 2000 Hz. Once the SNL was added, the STL peak was further accentuated but the subsequent STL dip remained unchanged. When comparing STL data for the two metamaterial panels ($Design1$ and $Design2$), it is evident that the proposed approach to establish acoustic barrier systems with high specific STL can only be successful if the mass ratio between cell interior and cell exterior is high, such as in panel $Design2$. For the lower mass ratio value in $Design1$, in particular, it was not possible to realize the desired STL peak. For this reason, in the remainder of this paper data is reported only for panel $Design2$.

A key challenge in the design of barrier materials is to create material system embodiments that possess STL's exceeding those of the σ-equivalent limp panel. For the panel $Design2$ with the SNL in a diffuse sound field, Fig. 9, the measured STL exceeds the (predicted) STL_d of the σ-equivalent limp panel in a diffuse field and reaches the (predicted) STL_n in a normally incident field. Once a normally incident sound field was considered, the measured STL for this barrier was found to exceed that of the (predicted) STL_n, Fig. 10, by around 4 dB. The normal incidence sound field was found to further enhance the resonance response of the metamaterial panel.

From the viewpoint of an engineering application of metamaterial panel the results presented so far demonstrate that the mass-efficient sound transmission loss characteristics of the cellular panels can be realized through configurations having high mass contrast (μ) and a high degree of normal-

ity of the incident sound field (achieved through the sound source itself and through a SNL). While obtaining an increased STL in a particular frequency range is often the primary design objective, it is also important to address the corresponding STL loss occurring in the dip region. High frequency sound can be effectively managed by the use of porous materials, such as fiber mats. Figure 11 shows the measured STL values for a configuration in which a SAL was added to the rear surface of the panel *Design*2 with the SNL on the incident side. The hybrid metamaterial panel possesses an areal mass $\sigma = 6.18$ kg/m^2. The measured sound transmission loss was compared to the analytically calculated $\mathrm{STL_d}$ for an areal mass-equivalent limp panel. Two areal mass values are considered, one ignoring the equivalent areal mass of the SNL (leading to an equivalent limp panel with 6.18 kg/m^2) and one including the equivalent areal mass of the SNL (leading to an equivalent limp panel with 7.74 kg/m^3). It can be observed that the $\mathrm{STL_d}$ was significantly improved compared to either of the equivalent limp panels in the STL peak region. The $\mathrm{STL_d}$ in the dip region was substantially increased through the addition of the SAL and does not fall below the STL of the limp panel. Overall, the $\mathrm{STL_d}$ of the HMP is a significant improvement over its σ-equivalent limp panel, particularly in the peak region. The $\mathrm{STL_d}$ of the HMP at any frequency including the dip frequency is at least equal to or higher than its σ-equivalent limp panel.

Finally, Fig. 12 compares the experimentally observed $\mathrm{STL_d}$ of the HMP and the HCP. The HCP comprises the reference limp panel in combination with SNL and SAL. The HCP possesses an areal-mass of $\sigma = 6.59\,\mathrm{kg/m^2}$ (6.6

percent higher than the HMP). From this result, it can be seen that HMP only performs better than a HCP in a region around the anti-resonance: at 1400 Hz the STL_d for the HMP is about 5 dB higher than that of the HCP. It can also be seen that the STL of the HMP is higher than or at least the same value as that of HCP for all the frequencies below 1400 Hz despite the 6 percent lower areal mass compared to the HCP. Sound treatment solutions like the one defined here may be very useful when the frequency of the noise source is stationary and narrow, such as, for example, the sound radiation from electrical transformers.

In the design of sound barrier systems, numerical simulations should ideally guide the processes as this approach would reduce the number of costly experiments. For the case of normally incident sound, Fig. 13 compares the measured STL data for the cellular panel $Design2$ with the SNL to the numerical prediction of STL from the finite element model. The occurrence of the peak and dip in the measured sound transmission loss data was bracketed by the numerical predictions considering models with the values for the cell interior plate thickness $mean(t_p) - stdev(t_p)$ and $mean(t_p) + stdev(t_p)$. The simulation considering a cell interior plate thickness $mean(t_p)+stdev(t_p)$ overestimated the critical frequency. For all numerical simulations, the actual STL peak and dip values were much more pronounced that those appearing in the experimental data. The difference between the experimentally observed behavior from numerical prediction had several causes. First, the numerical simulation was based on a single unit cell subjected to a normally incident sound field with the application of periodic boundary conditions; in contrast,

the experiments featured a panel having multiple unit cells (18×18) subjected to a sound field that was not of pure normal incidence. Secondly, there was a thickness variation among the unit cells of the machined test panel owing to the variation in the stock material thickness and machining error those resulting in the spread of the flexural resonances of individual unit cells over a wider band than ideally anticipated

V. Conclusions

In this study, the acoustic performance of a full-scale metamaterial barrier system was considered. The metamaterial panel consisted of an array of square cells with a plate-type cell interior and surrounding walls.

It was found that for a diffuse incidence sound field the STL performance of the planar cellular metamaterial panel was substantially reduced compared to the predicted normal incidence behavior. Yet, it was demonstrated that the performance of the cellular metamaterial panel can be improved by the addition of a sound normalizing layer to the front of the panel. That layer constrains the incident sound field to approach the panel at normal incidence. Further, the cellular metamaterial panel performance in the STL dip region can be improved by the addition of a sound absorbing layer to the transmission side. That layer has the effect of compensating for the reduction in transmission loss in the frequency range immediately above the metamaterial's peak transmission loss. Such an addition ensures that the performance of the metamaterial barrier system is at least equal to or sub-

stantially greater than an areal mass-equivalent limp panel over the entire the frequency range of interest. The effectiveness of cellular metamaterial barriers for sound transmission loss applications was found to depend significantly on the grid to wall mass ratio: that quantity not only determines the anti-resonance frequency, but also the degree of the STL amplification at that frequency.

Acknowledgements

The authors gratefully acknowledge the financial support provided by the United States Air Force Office of Scientific Research through the grant FQ8671-090162 and by the Purdue Research Foundation TRASK Fund.

References

[1] J. Wilby, Aircraft interior noise, Journal of Sound and Vibration 190 (3) (1996) 545–564.

[2] G. Jackson, H. Leventhall, Household appliance noise, Applied Acoustics 8 (2) (1975) 101–118.

[3] F. J. Fahy, P. Gardonio, Sound and Structural Vibration: Radiation, Transmission and Response, 2nd Edition, 633 p., Academic Press, Oxford, UK, 2007.

[4] Z. Y. Liu, X. X. Zhang, Y. W. Mao, Y. Y. Zhu, Z. Y. Yang, C. T. Chan, P. Sheng, Locally resonant sonic materials, Science 289 (5485) (2000) 1734–1736.

[5] E. C. Wester, X. Brémaud, B. Smith, Meta-material sound insulation, Building Acoustics 16 (2009) 21–30.

[6] Z. Yang, J. Mei, M. Yang, N. H. Chan, P. Sheng, Membrane-type acoustic metamaterial with negative dynamic mass, Physical Review Letters 101 (20) (2008) 204301.

[7] C. J. Naify, C. M. Chang, G. McKnight, S. Nutt, Transmission loss and dynamic response of membrane-type locally resonant acoustic metamaterials, Journal of Applied Physics 108 (11) (2010) 114905.

[8] Y. Xiao, J. Wen, X. Wen, Sound transmission loss of metamaterial-based thin plates with multiple subwavelength arrays of attached resonators, Journal of Sound and Vibration 331 (2012) 5408–5423.

[9] S. Varanasi, J. S. Bolton, T. Siegmund, R. J. Cipra, The low frequency performance of metamaterial barriers based on cellular structures, Applied Acoustics 74 (4) (2013) 485–495.

[10] P. A. Deymier (Ed.), Acoustic Metamaterials and Phononic Crystals, Vol. 173 of Solid-State Sciences, Springer, 2013.

[11] K. M. Ho, Z. Yang, X. X. Zhang, P. Sheng, Measurements of sound transmission through panels of locally resonant materials between impedance tubes, Applied Acoustics 66 (7) (2005) 751–765.

[12] Z. Yang, H. M. Dai, N. H. Chan, G. C. Ma, P. Sheng, Acoustic metamaterial panels for sound attenuation in the 50-1000 Hz regime, Applied Physics Letters 96 (4) (2010) 041906.

[13] C. J. Naify, C.-M. Chang, G. McKnight, S. Nutt, Transmission loss of membrane-type acoustic metamaterials with coaxial ring masses, Journal of Applied Physics 110 (12) (2011) 124903.

[14] C. J. Naify, C.-M. Chang, G. McKnight, F. Scheulen, S. Nutt, Membrane-type metamaterials: Transmission loss of multi-celled arrays, Journal of Applied Physics 109 (10) (2011) 104902.

[15] Y. Zhang, J. Wen, H. Zhao, D. Yu, L. Cai, X. Wen, Sound insulation property of membrane-type acoustic metamaterials carrying different masses at adjacent cells, Journal of Applied Physics 114 (6) (2013) 063515.

[16] ASTM Standard E2611-09, 2009, Standard test method for measurement of normal incidence sound transmission of acoustical materials based on the transfer matrix method, ASTM International, West Conshohocken, PA, 2009.

[17] J. S. Bolton, T. Yoo, O. Olivieri, Measurement of normal incidence transmission loss and other acoustical properties of materials placed in a standing wave tube, Tech. Rep. 1, Brüel and Kjær, Naerum, Denmark, (2007).

[18] B. H. Song, J. S. Bolton, A transfer-matrix approach for estimating the characteristic impedance and wave numbers of limp and rigid porous materials, Journal of the Acoustical Society of America 107 (3) (2000) 1131–1152.

[19] S. H. Lee, C. M. Park, Y. M. Seo, Z. G. Wang, C. K. Kim, Composite acoustic medium with simultaneously negative density and modulus, Physical Review Letters 104 (5) (2010) 054301.

[20] S. H. Lee, C. M. Park, Y. M. Seo, Z. G. Wang, C. K. Kim, Acoustic metamaterial with negative modulus, Journal of Physics: Condensed Matter 21 (17) (2009) 175704.

[21] S. H. Lee, C. M. Park, Y. M. Seo, Z. G. Wang, C. K. Kim, Acoustic metamaterial with negative density, Physics Letters A 373 (48) (2009) 4464–4469.

[22] L. Chalmers, D. Elford, F. Kusmartsev, G. Swallowe, Acoustic band gap formation in two-dimensional locally resonant sonic crystals comprised of Helmholtz resonators, International Journal of Modern Physics B 23 (20n21) (2009) 4234–4243.

[23] A. Pellicier, N. Trompette, A review of analytical methods, based on the wave approach, to compute partitions transmission loss, Applied Acoustics 68 (10) (2007) 1192–1212.

[24] B. Assouar, M. Oudich, X. Zhou, Sound insulation and energy harvesting based on acoustic metamaterial plate, in: SPIE Smart Structures and Materials+Nondestructive Evaluation and Health Monitoring, International Society for Optics and Photonics, 2015, pp. 94380U–94380U.

[25] A. Hall, E. P. Calius, G. Dodd, K. Chan, Development of locally resonant structures for sonic barriers, in: SPIE Smart Structures and Materials + Nondestructive Evaluation and Health Monitoring, International Society for Optics and Photonics, 2013, pp. 86953M–86953M.

[26] M. P. Waser, M. J. Crocker, Introduction to the two-microphone cross-spectral method of determining sound intensity, Noise Control Engineering Journal 22 (3) (1984) 76–85.

[27] J. S. Bolton, N.-M. Shiau, Y. Kang, Sound transmission through multi-panel structures lined with elastic porous materials, Journal of Sound and Vibration 191 (3) (1996) 317–347.

[28] ASTM Standard E2249, 2016, Standard test method for laboratory measurement of airborne transmission loss of building partitions and elements using sound intensity, ASTM International, West Conshohocken, PA, 2016.

[29] S. Varanasi, J. Bolton, T. Siegmund, Random incidence transmission loss of a metamaterial barrier system, in: INTER-NOISE and NOISE-CON Congress and Conference Proceedings, Vol. 249, Institute of Noise Control Engineering, 2014, pp. 5594–5601.

[30] L. E. Kinsler, A. R. Frey, A. B. Coppens, J. V. Sanders, Fundamentals of Acoustics, Chapter 9, 4th Edition, Wiley, New York, 1999.

[31] F. Jacobsen, V. Cutanda, P. M. Juhl, A numerical and experimental investigation of the performance of sound intensity probes at high frequencies, The Journal of the Acoustical Society of America 103 (2) (1998) 953–961.

[32] SIMULIA, Inc., Providence, RI, USA, ABAQUS 6.10 Documentation (May 2010).

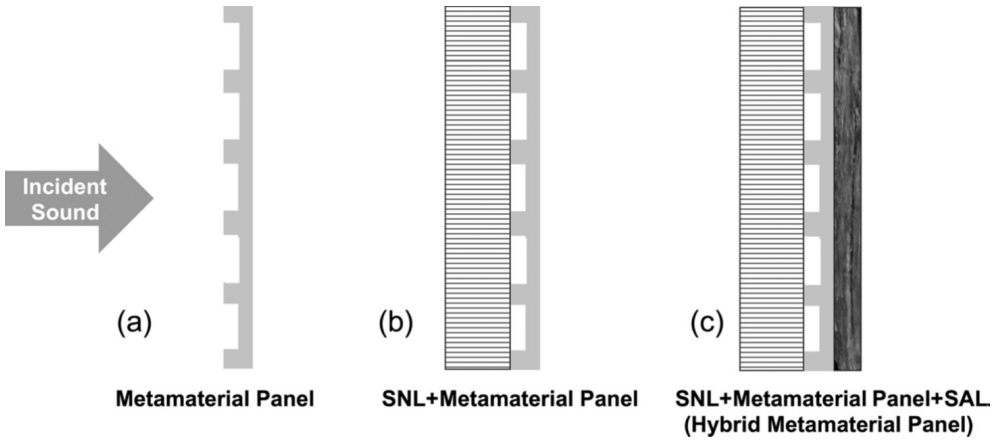

Figure 1: Schematics of the cellular metamaterial based systems: (a) Cellular metamaterial panel alone, (b) Cellular metamaterial panel with the sound normalizing layer (SNL), and (c) hybrid metamaterial panel (HMP) comprised of sound normalizing layer (SNL), cellular panel core and sound absorbing layer (SAL).

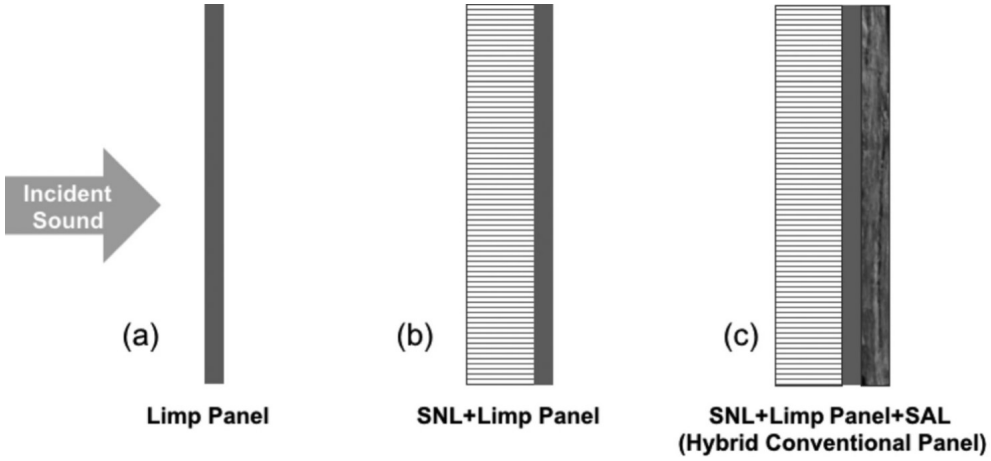

Figure 2: Schematics of the reference limp panels systems: (a) Reference limp panel alone, (b) Reference limp panel with sound normalizing layer (SNL), and (c) hybrid conventional panel (HCP) comprised of sound normalizing layer (SNL), reference limp panel core and sound absorbing layer (SAL).

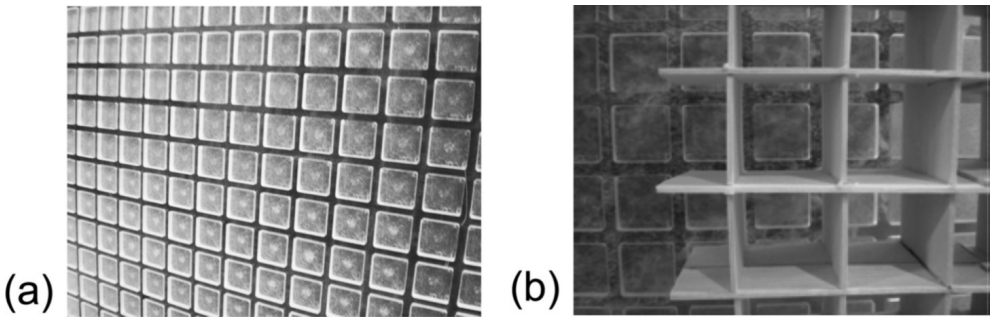

Figure 3: Photographs of (a) cellular panel, (b) assembly of sound normalizing layer (SNL), cellular panel, and sound absorbing layer (SAL).

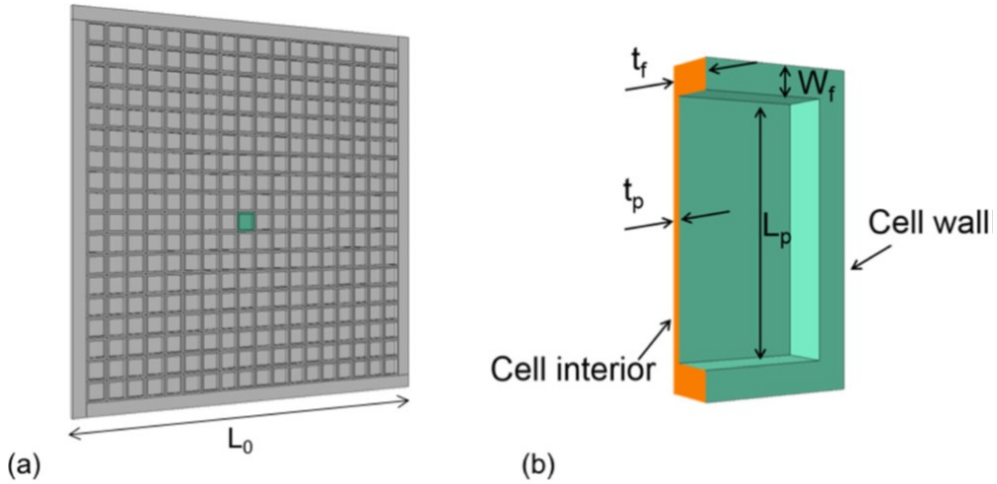

Figure 4: (a) A schematic of the cellular metamaterial panel. (b) A cut-section of the unit cell with the dimensions L_p: Edge length of the cell interior, t_p: Thickness of the cell interior, W_f: Width of the cell wall and t_f: Thickness of the cell wall.

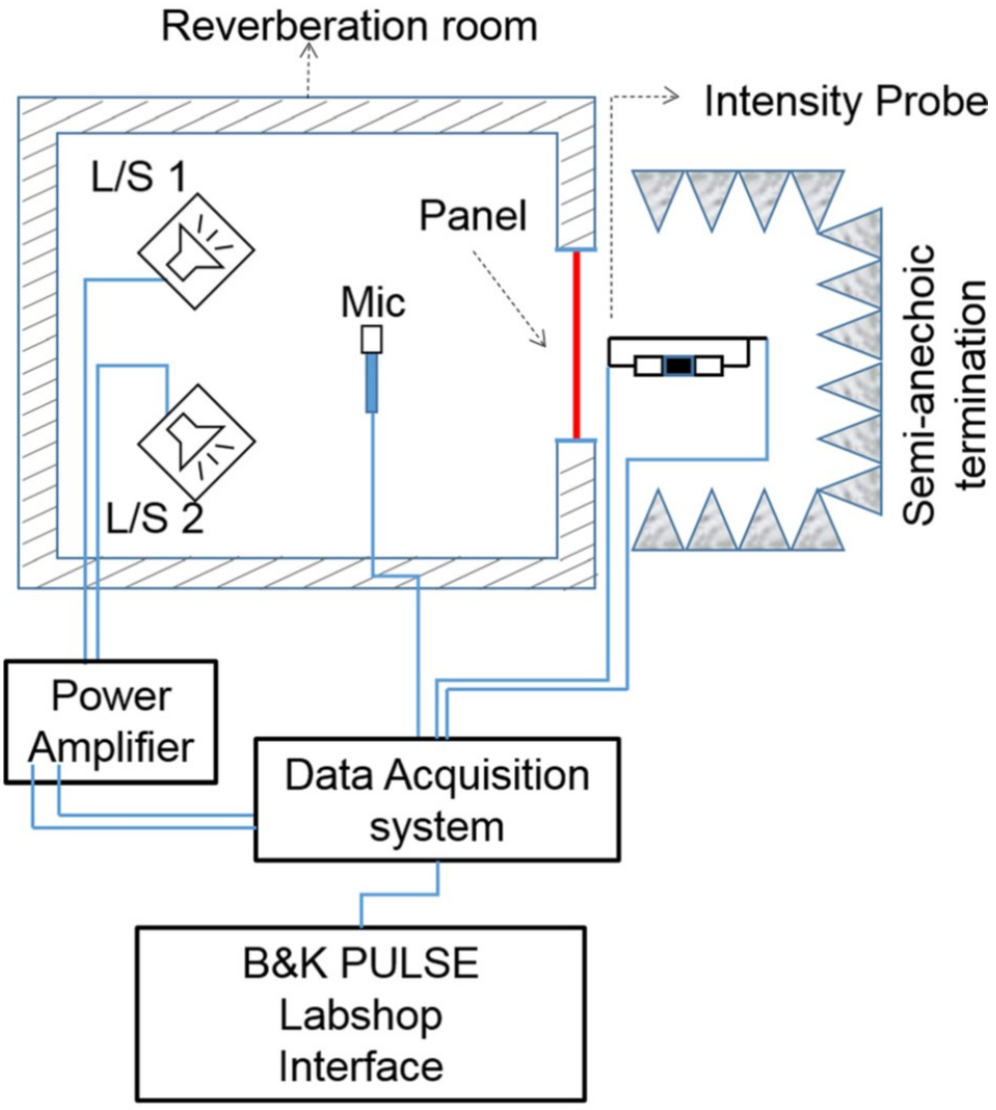

Figure 5: A schematic of the reverberation room setup for experiments with a predominantly diffuse sound field.

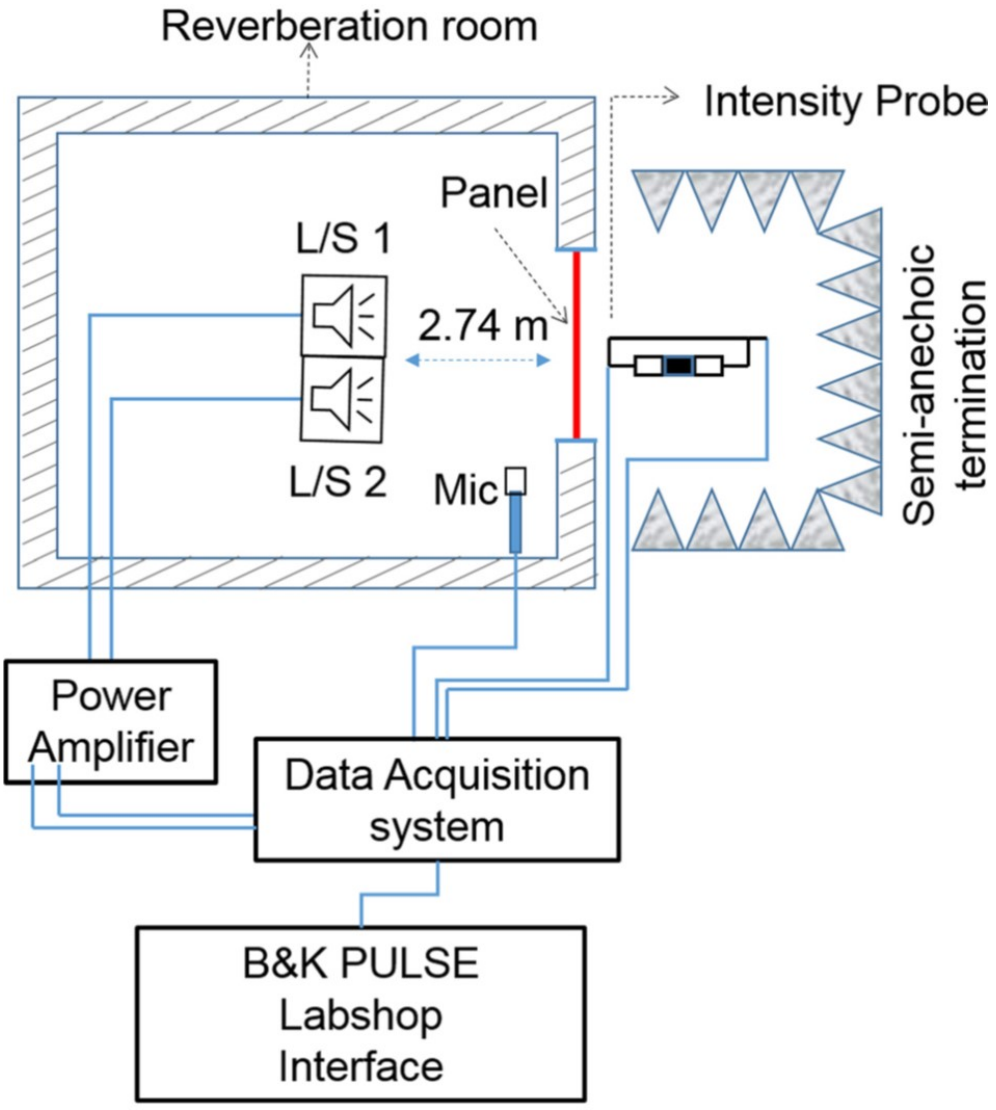

Figure 6: A schematic of the reverberation room setup for experiments with a predominantly normally incident sound field.

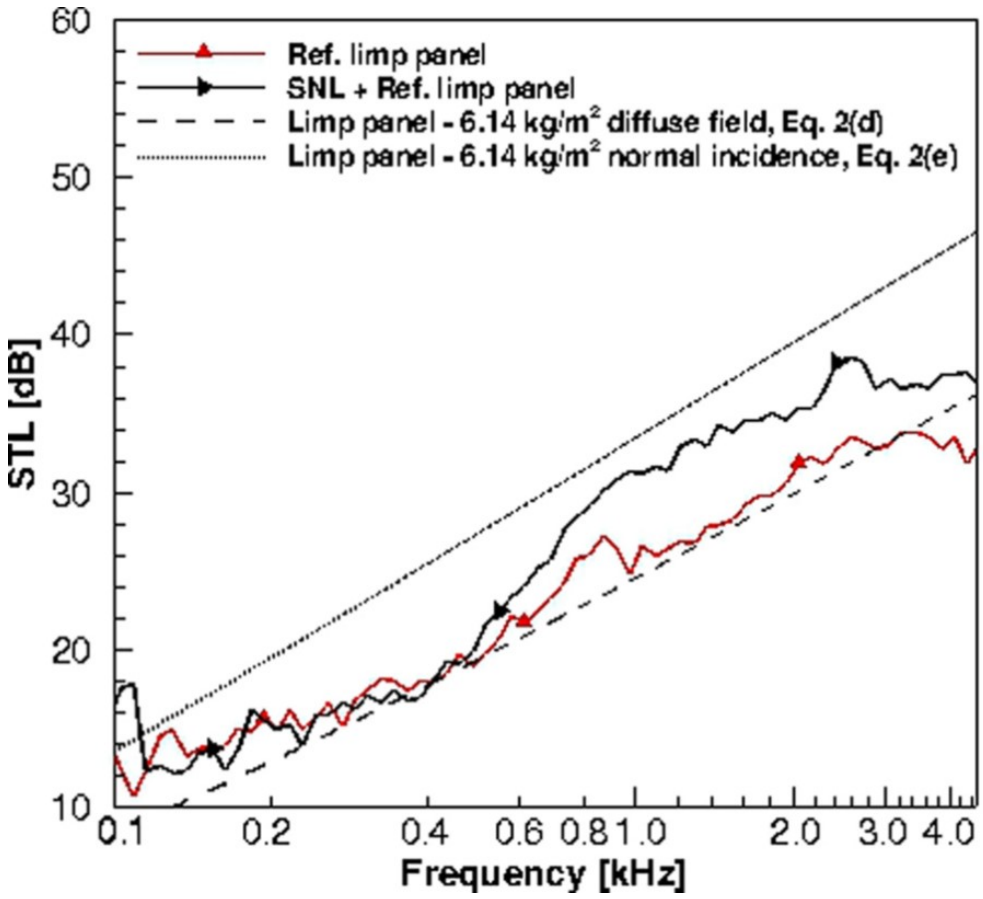

Figure 7: Measured STL of the bare reference limp panel and the reference limp panel with SNL, diffuse sound field. Comparison to the analytical solutions of $\mathrm{STL_d}$ and $\mathrm{STL_n}$.

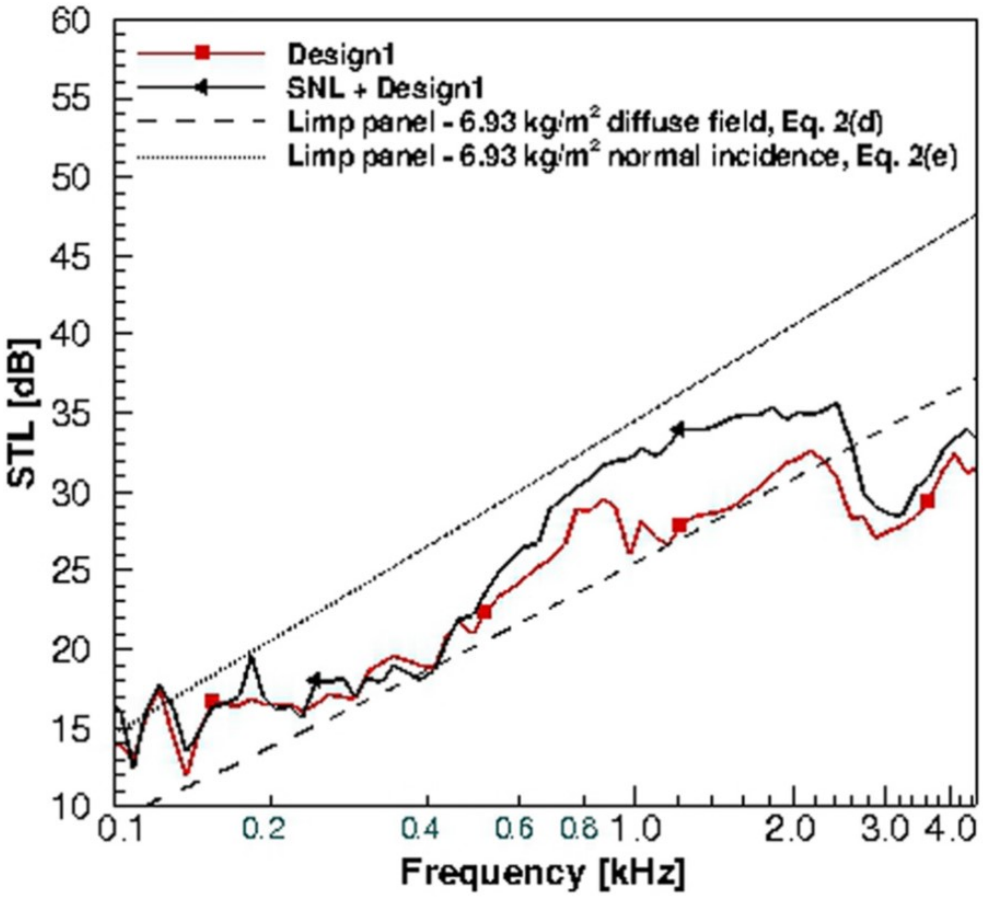

Figure 8: Measured STL of bare cellular metamaterial panel *Design*1 and the panel with SNL, diffuse sound field. Comparison to the analytical solutions $\mathrm{STL_d}$ and $\mathrm{STL_n}$ for a σ-equivalent limp panel.

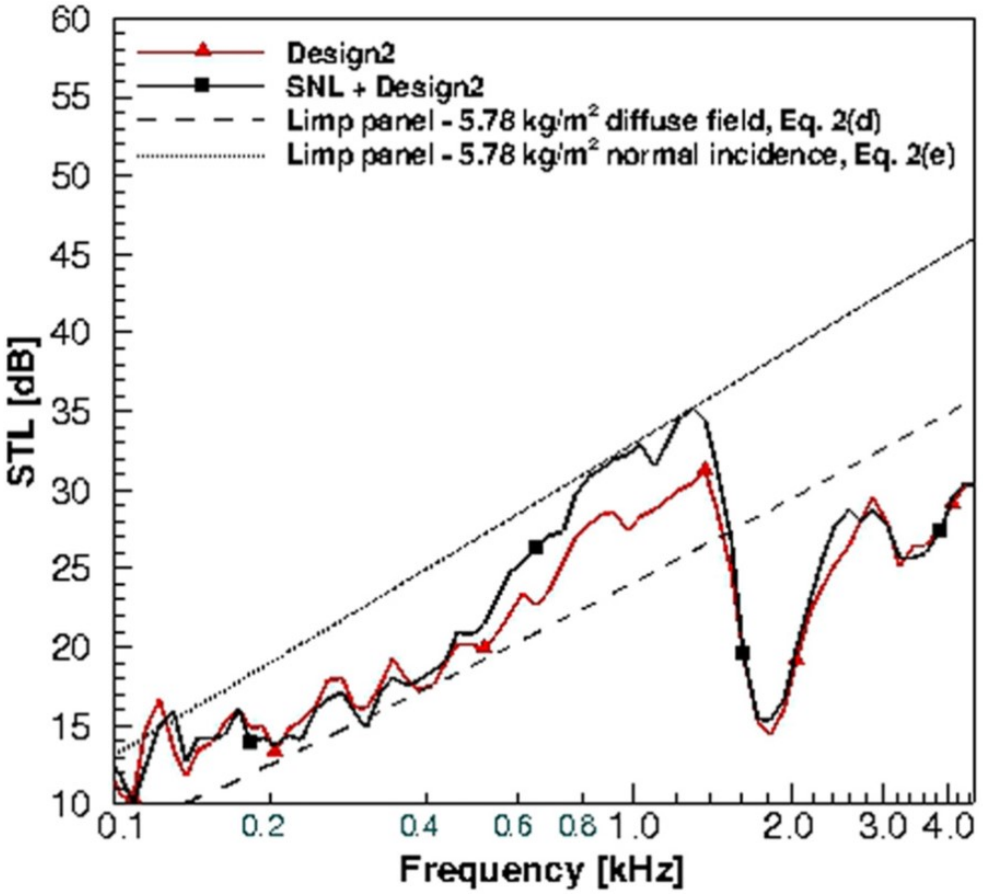

Figure 9: Measured STL of cellular metamaterial panel *Design*2 and the panel with SNL, diffuse sound field. Comparison to analytical solutions for $\mathrm{STL_d}$ and $\mathrm{STL_n}$ for a σ-equivalent limp panel.

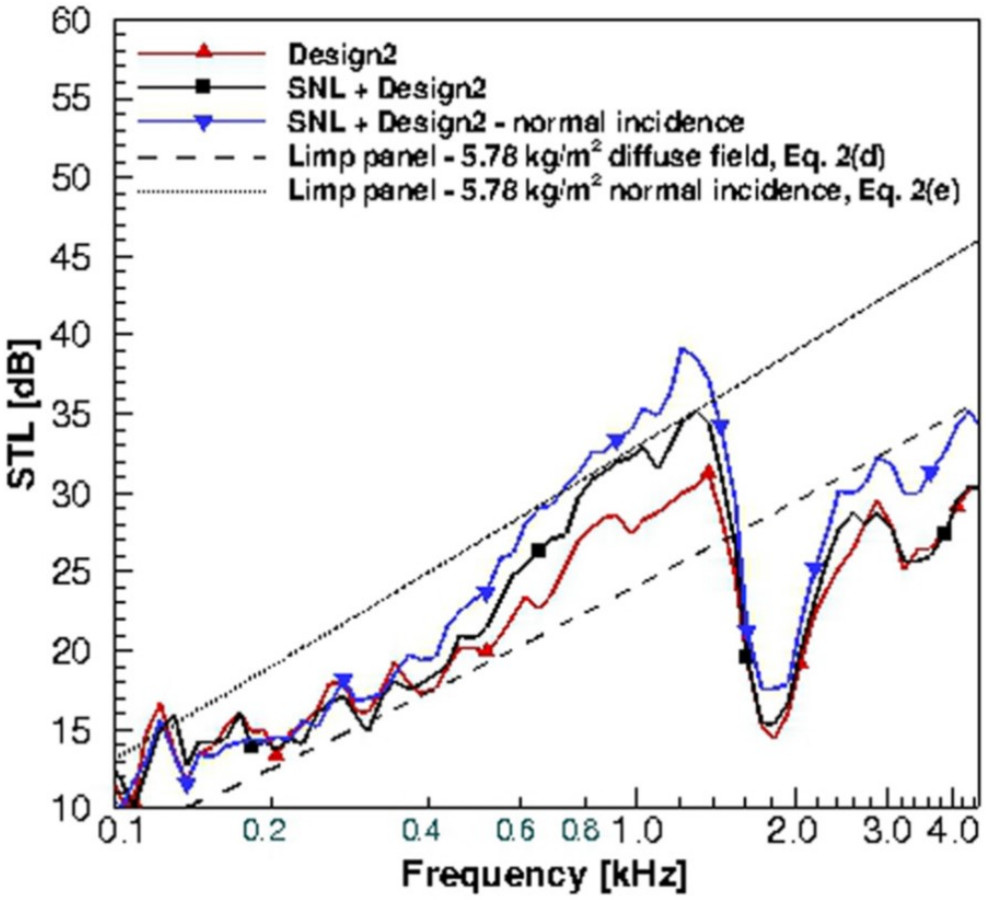

Figure 10: Measured STL of the cellular metamaterial panel *Design*2 with SNL in a normally incident sound field, compared to the STL of the bare metamaterial panel *Design*2 and the panel with SNL exposed to a diffuse incident sound field. Comparison to analytical solutions for $\mathrm{STL_d}$ and $\mathrm{STL_n}$ for a σ-equivalent limp panel.

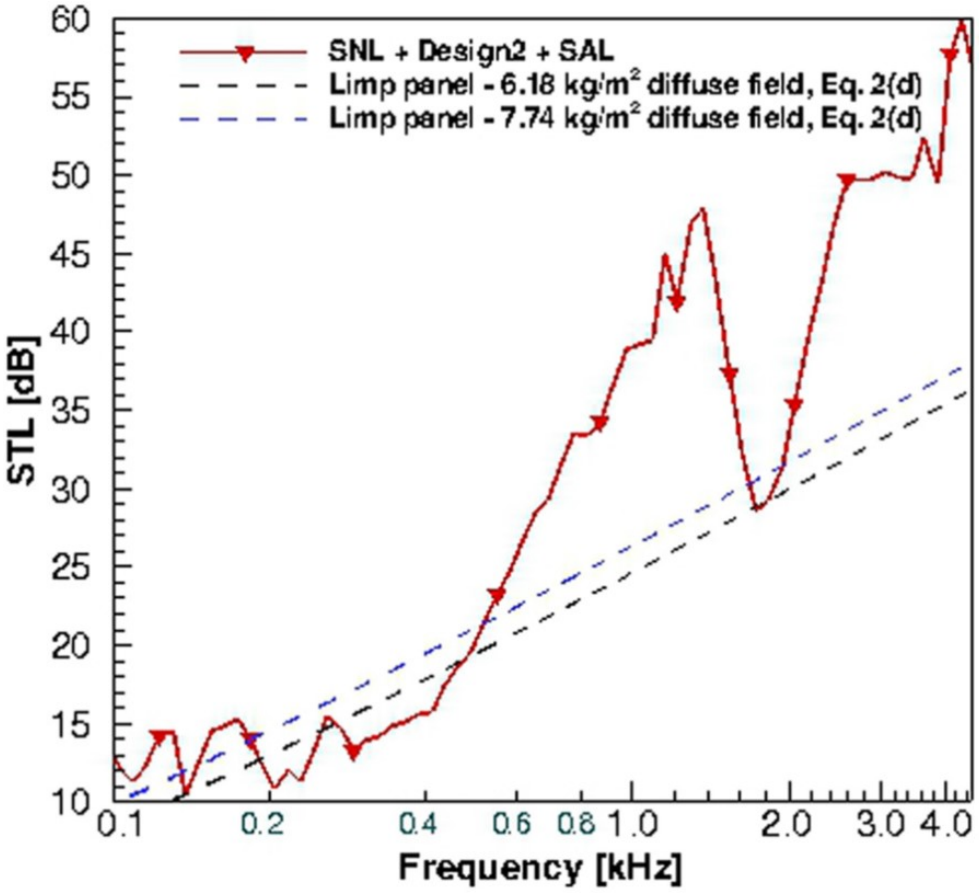

Figure 11: Measured STL of the hybrid metamaterial panel (HMP) in a diffuse sound field, compared against the analytical solution for $\mathrm{STL_d}$ for a σ-equivalent limp panel.

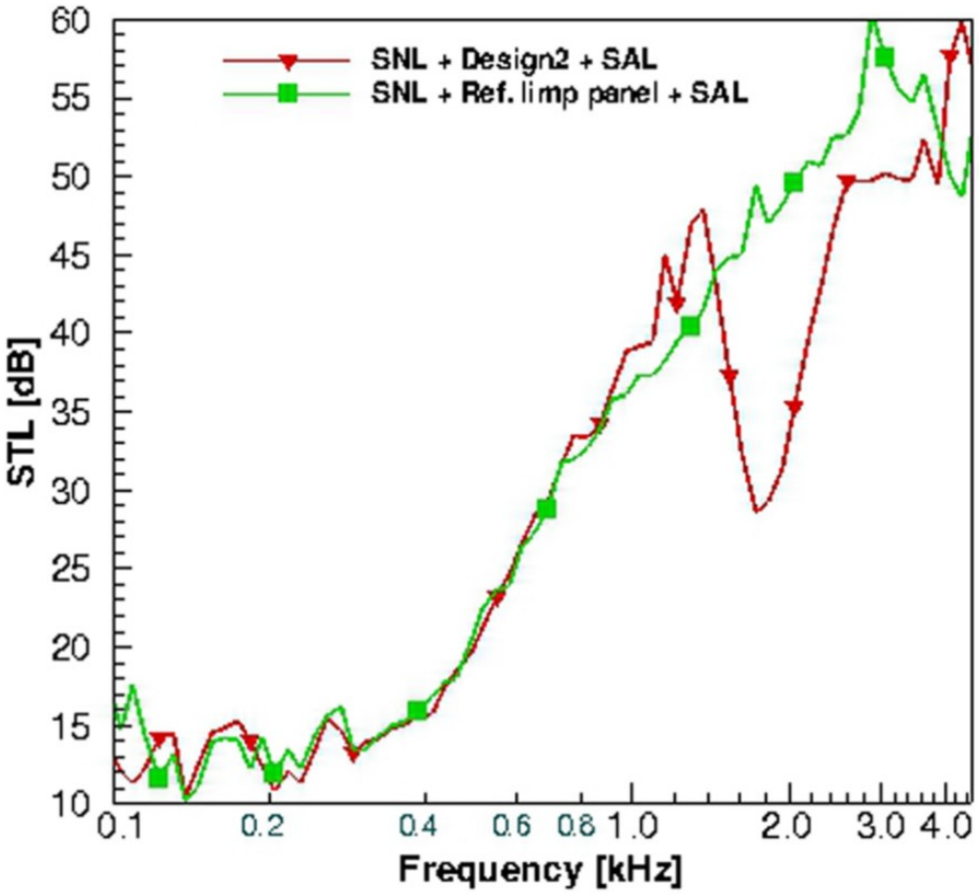

Figure 12: Comparison of the measured STL of HMP and HCP, diffuse sound field.

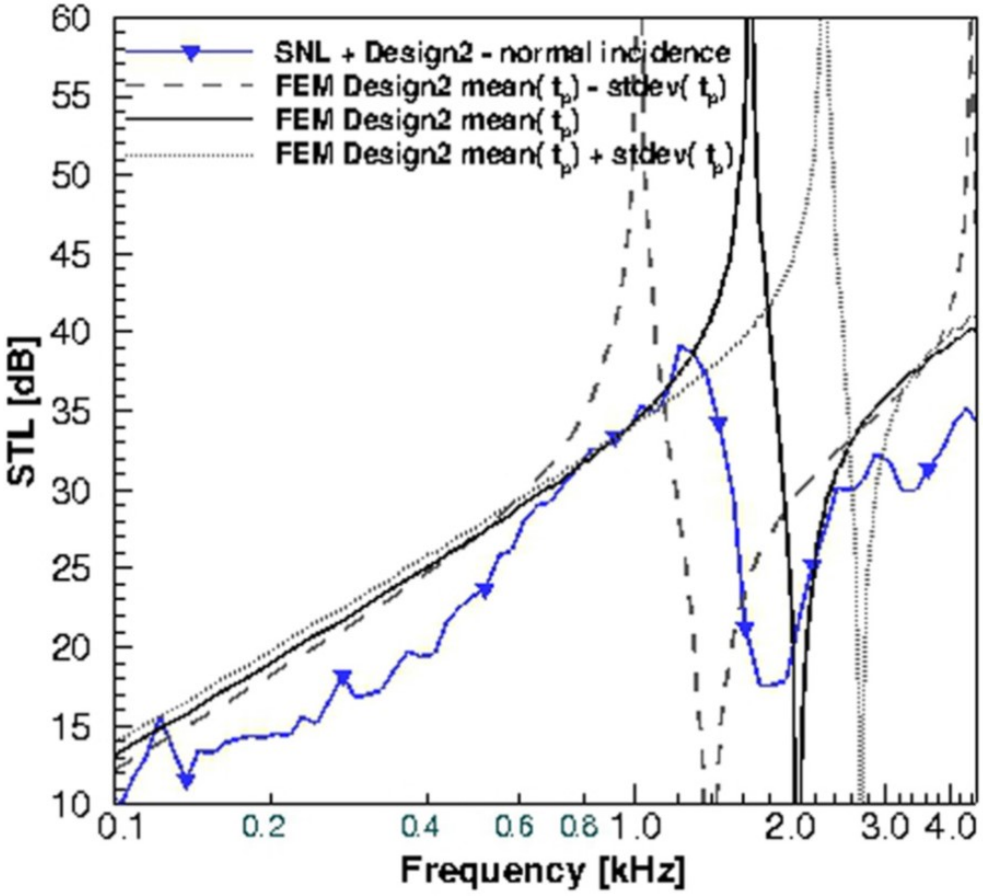

Figure 13: Measured STL of the cellular metamaterial panel *Design*2 with SNL exposed to a normally incident sound field compared against the numerically predicted STL using the computational unit cell model (considering three different thickness values for the unit cell interior).

A Appendix: Finite Element Model of the Unit Cell

The model consisted of two acoustic domains (upstream and downstream) and a solid domain consisting of a unit cell separating the two acoustic domains. The acoustic domains in the model were given a square cross-section with dimensions of L_p+2W_f by L_p+2W_f, thus exposing the complete unit cell to a normally incident sound field. The edges of the unit cells were subjected to periodic boundary conditions: $u_1|_{x_1=-(L_p/2+W_f)} = u_1|_{x_1=(L_p/2+W_f)} = 0$ and $u_2|_{x_2=-(L_p/2+W_f)} = u_2|_{x_2=(L_p/2+W_f)} = 0$, where x_1, x_2 are the in-plane coordinates: Fig. 14. Also, u_1, u_2 are the displacement fields in the x_1 and x_2 directions, respectively. The lengths of the up- and downstream acoustic domains were taken to be 500.0 mm each. Acoustical elements (8-node linear hexahedral) were used to discretize the acoustical domains, while structural elements (20-node quadratic hexahedral, reduced integration) were used to discretize the solid domain. The element size in the acoustic domain was chosen to conform to the rule that there should be more than six elements per wavelength at the highest frequency in the range considered. In the unit cell, the element size was so chosen to capture the flexural behavior as well as the dynamic behavior. A minimum of three layers of elements were used through the thickness (t_p) of the plate representing the cell interior to satisfy the former requirement, and the element sizes were also chosen so that there were at least six elements in one shear wavelength at the highest frequency considered to ensure the latter.

A sound source radiating a single frequency sound pressure was located at the upstream end of the acoustic domain while the downstream end of the acoustic domain was given an anechoic termination by imposing a specific acoustic impedance of $\rho_0 c$: i.e., the characteristic impedance of air. Here, ρ_0 is the density of air and c is the speed of sound in air. The model was executed one-frequency-at-a-time with a frequency interval of 20 Hz to cover a specified frequency $(0 - 5000$ Hz) range with a unit amplitude input.

To evaluate the characteristics of the unit cell, predicted sound pressures were recorded by virtual "microphones" at two axial locations in both the upstream and downstream acoustic domains at each frequency within the specified range $(0 - 5000$ Hz). The transfer functions between the first microphone and the other three microphones were determined using the single load method and were then used to evaluate the sound transmission loss characteristics of the unit cell [17, 18]. The pressure measurement locations were chosen so that they were at least a distance $L_p + 2W_f$ away from the unit cell on either side. The independence of the results on the choice of pressure measurement locations was confirmed by processing data obtained from different sets of measurement pairs for the same model.

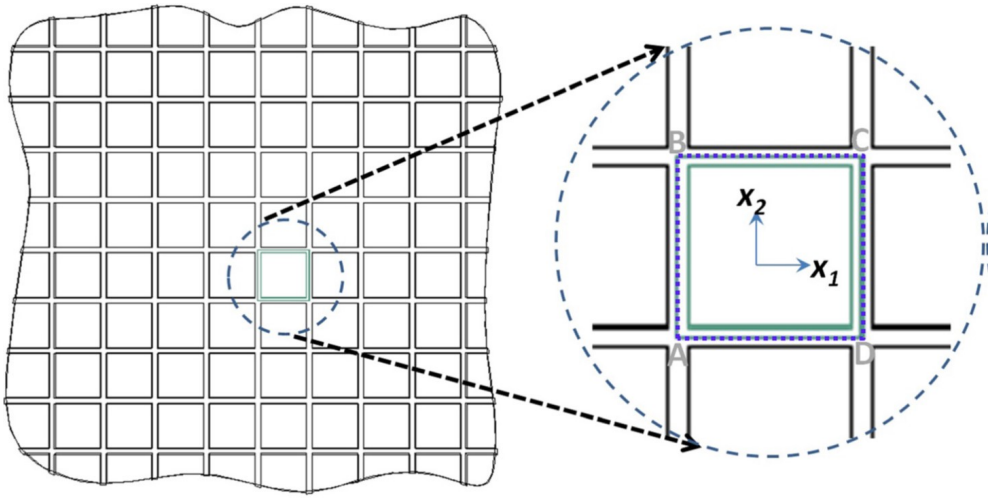

Figure 14: A normal view of the cellular panel illustrating the periodic boundary conditions on a unit cell. In the magnified view of a unit cell, the periodic boundary conditions are imposed on the edges marked as $ABCD$ (shown as dotted lines) with $u_1 = 0$ on AB and DC, and $u_2 = 0$ on AD and BC.